

Quantum quenches and thermalization in one-dimensional fermionic systems

Marcos Rigol

Department of Physics, Georgetown University, Washington, DC 20057, USA

We study the dynamics and thermalization of strongly correlated fermions in finite one-dimensional lattices after a quantum quench. Our calculations are performed using exact diagonalization. We focus on one- and two-body observables such as the momentum distribution function $n(k)$ and the density-density structure factor $N(k)$, respectively, and study the effects of approaching an integrable point. We show that while the relaxation dynamics and thermalization of $N(k)$ for fermions is very similar to the one of hardcore bosons, the behavior of $n(k)$ is distinctively different. The latter observable exhibits a slower relaxation dynamics in fermionic systems. We identify the origin of this behavior, which is related to the off-diagonal matrix elements of $n(k)$ in the basis of the eigenstates of the Hamiltonian. More generally, we find that thermalization occurs far away from integrability and that it breaks down as one approaches the integrable point.

PACS numbers: 03.75.Ss, 05.30.Fk, 02.30.Ik, 67.85.Lm

I. INTRODUCTION

In recent years, the study of the nonequilibrium dynamics of isolated quantum systems has attracted a great deal of attention. The main motivation for these studies lies behind the spectacular success that experimentalists have achieved in trapping and manipulating ultracold quantum gases. This has allowed them to, for example, load ultracold bosons in optical lattices and study the collapse and revival of the matter wave interference after quenching the interaction strength from deep in the superfluid regime into deep in the Mott insulating regime [1], and to observe the damping of the dipole oscillations when the center of mass of the gas was displaced away from the center of the trap [2–4].

Since these atomic gases are trapped, cooled, and manipulated in a very high vacuum, i.e., in no contact with any kind of thermal or particle reservoir, a fundamental question that arises is whether after a sudden perturbation the system will relax to thermal equilibrium (an equilibrium in which observables are described by standard statistical mechanical ensembles). The usual assumption is that thermalization occurs in general. However, recent experiments in one-dimensional (1D) geometries (created by a deep two-dimensional optical lattice) have failed to observe relaxation to a thermal distribution after a quench [5]. The absence of thermalization can be understood in the very special regime in which the system is at an integrable point [6]. Interestingly, in Ref. [5] the gas was perturbed away from integrability and thermalization did not occur. Other experiments in 1D geometries (generated by an atom chip) have reported the indirect observation of thermalization [7]. In the latter case, the transverse confinement was not as strong as the one induced by the optical lattice in Ref. [5]. The question of whether strict one dimensionality could affect the outcome of the relaxation dynamics has not been fully addressed experimentally.

The particular case in which the system is at an integrable point lends itself to combined analytical and numerical studies, which have allowed theorists to show that in that case the relaxation dynamics after a quench lead to nonthermal equilibrium distributions of few-body observables [6]. In addition, a generalization of the Gibbs ensemble, which takes into

account the conserved quantities that make the system integrable, has been shown to successfully describe experimental observables after relaxation [6, 8]. Further analytical and numerical works have analyzed the relevance of the generalized Gibbs ensemble to different models and observables and addressed its limits of applicability [9–18].

When the systems are far away from integrability, for example in higher dimensions, the expectation is that they should thermalize. Recent numerical work has shown this to be the case for bosons in two dimensions, studied with exact diagonalization [19], and for fermions studied within the dynamical mean-field theory (DMFT) approximation [20]. In addition, thermalization in the isolated two-dimensional bosonic case could be understood within the eigenstate thermalization hypothesis (ETH) proposed by Deutsch [21] and Srednicki [22], in which the individual eigenstates of the many-body Hamiltonian exhibit thermal behavior [19].

In one-dimensional nonintegrable systems, the situation is a bit more subtle as many models can be tuned (by changing some Hamiltonian parameters) to be arbitrarily close to integrable points. An early study of the relaxation dynamics in fermionic systems when breaking integrability, using time-dependent density renormalization group (tDMRG) [23], concluded that thermalization does not occur even if the system is perturbed away from the integrable point. Another early work in 1D, also using tDMRG, studied the relaxation dynamics of the (nonintegrable) Bose-Hubbard model when quenching the system across the superfluid-to-Mott-insulator transition [24]. In that case the authors concluded that thermalization occurs in some regimes but not in others.

More recently, we have performed a systematic study of thermalization in finite 1D systems of hardcore bosons. Our results indicate that far away from integrability the system does thermalize [25]. However, thermalization breaks down as one approaches the integrable point. An important question that still needs to be answered is what happens with the point at which thermalization breaks down as one approaches the thermodynamic limit. It may either move toward the integrable point or toward some point away from integrability. More powerful numerical techniques or analytical approaches may be required to answer that question, which will not be addressed here.

In this work, we extend the analysis in Ref. [25] to the fermionic case, which allows us to discuss some of the issues that remained open in Ref. [23]. In particular, the time scales required for different observables to relax to a stationary “equilibrium” distribution, and the description of the observables after relaxation. We also study how the closeness to an integrable point affects the dynamics and thermalization after a quantum quench. As in earlier works [19, 25], we show that the breakdown of thermalization for our observables is directly linked to the breakdown of ETH.

The presentation is organized as follows. In Sec. II, we introduce the lattice model to describe 1D fermions with nearest- and next-nearest-neighbor hopping and repulsive interactions. We define our observables of interest and briefly discuss our numerical approach. The nonequilibrium dynamics of this model is presented in Sec. III. Section IV is devoted to the analysis of statistical mechanical approaches to describe observables after relaxation. In Sec. V, we justify these statistical mechanical approaches, or their failure, within ETH. An explanation of why the momentum distribution function of the fermions has a distinctively slow relaxation dynamics is presented in Sec. VI in terms of the off-diagonal elements of this observable in the basis of the eigenstates of the Hamiltonian. Finally, the summary and outlook are presented in Sec. VII.

II. HAMILTONIAN AND OBSERVABLES

The Hamiltonian of spin-polarized fermions in a 1D lattice with periodic boundary conditions can be written as

$$\hat{H} = \sum_{i=1}^L \left\{ -t \left(\hat{f}_i^\dagger \hat{f}_{i+1} + \text{H.c.} \right) + V \left(\hat{n}_i - \frac{1}{2} \right) \left(\hat{n}_{i+1} - \frac{1}{2} \right) - t' \left(\hat{f}_i^\dagger \hat{f}_{i+2} + \text{H.c.} \right) + V' \left(\hat{n}_i - \frac{1}{2} \right) \left(\hat{n}_{i+2} - \frac{1}{2} \right) \right\}. \quad (1)$$

where the fermionic creation and annihilation operators at site i are denoted by \hat{f}_i^\dagger and \hat{f}_i , respectively, and the local-density operator by $\hat{n}_i = \hat{f}_i^\dagger \hat{f}_i$. In Eq. (1), the nearest- and next-nearest-neighbor hopping parameters are denoted by t and t' , respectively, and the nearest- and next-nearest-neighbor interactions are denoted by V and V' , respectively. In our study, we only consider repulsive interactions ($V, V' > 0$), and the number of lattice sites is denoted by L .

In Ref. [25], we have already studied a very similar Hamiltonian for hardcore bosons (bosons with an infinite on-site repulsion), in which case

$$\hat{H}_b = \sum_{i=1}^L \left\{ -t \left(\hat{b}_i^\dagger \hat{b}_{i+1} + \text{H.c.} \right) + V \left(\hat{n}_i^b - \frac{1}{2} \right) \left(\hat{n}_{i+1}^b - \frac{1}{2} \right) - t' \left(\hat{b}_i^\dagger \hat{b}_{i+2} + \text{H.c.} \right) + V' \left(\hat{n}_i^b - \frac{1}{2} \right) \left(\hat{n}_{i+2}^b - \frac{1}{2} \right) \right\}. \quad (2)$$

where the hardcore boson creation and annihilation operators at site i are denoted by \hat{b}_i^\dagger and \hat{b}_i , respectively, and the local-density operator by $\hat{n}_i^b = \hat{b}_i^\dagger \hat{b}_i$. The parameters t , V , t' , and

V' in Eq. (2) have exactly the same meaning for hardcore bosons as for the fermions in Eq. (1). For hardcore bosons, the creation and annihilation operators commute as usual for bosons

$$[\hat{b}_i, \hat{b}_j^\dagger] = [\hat{b}_i, \hat{b}_j] = [\hat{b}_i^\dagger, \hat{b}_j^\dagger] = 0, \quad \text{for } i \neq j, \quad (3)$$

but on the same site, the hardcore bosons operators satisfy anticommutation relations typical of fermions,

$$\left\{ \hat{b}_i, \hat{b}_i^\dagger \right\} = 1, \quad \hat{b}_i^{\dagger 2} = \hat{b}_i^2 = 0. \quad (4)$$

These constraints avoid double or higher occupancy of the lattice sites.

Similar to the hardcore boson case studied in Ref. [25], the Hamiltonian (1) is integrable for $t' = V' = 0$. In this section, we restrict our analysis to systems with $1/3$ filling, and study the effects of finite, but small, values of $t' = V' \neq 0$ when one departs from the integrable point. In this case, the ground state of our Hamiltonian is always a Luttinger liquid and no metal-insulator transition occurs in the system [26].

For $t' = 0$, the fermionic Hamiltonian (1) can be mapped onto the identical Hamiltonian for hardcore bosons (2) (up to a boundary effect), i.e., the fermionic operators in Eq. (1) just need to be replaced by operators describing hardcore bosons. This can be done using the Jordan-Wigner transformation [27], and implies that in the thermodynamic limit both systems have the same spectrum and identical diagonal correlations. However, off-diagonal correlations and related observables, such as the momentum distribution function, are very different for fermions and bosons. A finite value of t' still allows for a mapping of the fermionic Hamiltonian (1) onto a Hamiltonian of hardcore bosons. However, the new hardcore boson Hamiltonian for $t' \neq 0$ will be different to the one in Eq. (2). The mapping introduces additional operators in the term proportional to t' . In addition, in the fermionic case, a finite value of t' breaks the particle-hole symmetry present for $t' = 0$ and present for any value of t' in the hardcore boson case.

The study of the nonequilibrium dynamics and thermodynamics of these systems is performed using full exact diagonalization of the Hamiltonian (1). For our largest system sizes, eight fermions in 24 sites, the total Hilbert space has dimension $D = 735\,471$. We take advantage of the translational symmetry of the lattice, which allows us to block diagonalize the full Hamiltonian while the dimension of the largest block (in k space) is $D_k = 30\,667$.

In this work, we focus our analysis on two observables. The first one in the momentum distribution function

$$\hat{n}(k) = \frac{1}{L} \sum_{i,j} e^{-k(i-j)} \hat{f}_i^\dagger \hat{f}_j, \quad (5)$$

which is the Fourier transform of the one-body density matrix ($\hat{\rho}_{ij} = \hat{f}_i^\dagger \hat{f}_j$). As mentioned before, this observable behaves very differently for fermions as compared with the hardcore bosons to which they can be mapped. We should add that $n(k)$ is usually measured in experiments with ultracold quantum gases via time-of-flight expansion.

The second observable of interest is the density-density structure factor

$$\hat{N}(k) = \frac{1}{L} \sum_{i,j} e^{-k(i-j)} \hat{n}_i \hat{n}_j, \quad (6)$$

which is the Fourier transform of the density-density correlation matrix. Since we work at fixed number of fermions N_f , the expectation value of $\hat{N}(k=0)$ is always $\langle \hat{N}(k=0) \rangle = N_f^2/L$ and, as usual, we set it to zero by subtracting that trivial constant. The structure factor can be measured in cold gases experiments by means of noise correlations [28].

III. NONEQUILIBRIUM DYNAMICS

We will restrict our study of the nonequilibrium dynamics to the case in which the system is taken out of equilibrium by means of a quench. Quenches are a special way to induce dynamics by starting with an eigenstate of some initial Hamiltonian \hat{H}_{ini} , and then instantaneously changing the Hamiltonian (at time $\tau = 0$) to some final time-independent Hamiltonian \hat{H}_{fin} .

As mentioned previously, our model is integrable for $t' = V' = 0$. Since we are interested in studying the effect that approaching an integrable point has on the dynamics and thermalization of the system, we take the initial state to be an eigenstate of a system with $t = t_{ini}$, $V = V_{ini}$, t' , V' , and then quench the nearest-neighbor parameters t and V to $t = t_{fin}$, $V = V_{fin}$ without changing t' , V' , i.e., we only change $t_{ini}, V_{ini} \rightarrow t_{fin}, V_{fin}$. This quench is performed for different values of t' , V' as one approaches the integrable point $t' = V' = 0$.

Notice that our quenches do not break translational symmetry. For that reason, we always select the initial state to be one of the eigenstates of the initial Hamiltonian in the total $k = 0$ sector. Since translational symmetry is preserved, only states with zero total momentum are required to calculate the exact time evolution of the system

$$|\psi(\tau)\rangle = e^{-i\hat{H}_{fin}\tau} |\psi_{ini}\rangle = \sum_{\alpha} C_{\alpha} e^{-iE_{\alpha}\tau} |\Psi_{\alpha}^0\rangle, \quad (7)$$

where $|\psi(\tau)\rangle$ is the time-evolving state, $|\psi_{ini}\rangle$ is the initial state, $|\Psi_{\alpha}^0\rangle$ are the eigenstates of the final Hamiltonian with zero total momentum, energy E_{α} , and $C_{\alpha} = \langle \Psi_{\alpha}^0 | \psi_{ini} \rangle$. The sum runs over all the eigenstates of the total $k = 0$ sector. In this section, we perform the exact time evolution of up to eight fermions in lattices with up to 24 sites. This means that the largest total $k = 0$ sector diagonalized had 30 666 states.

In contrast to classical systems, where one has to perform the time evolution in order to compute the long-time average of any observable, in isolated quantum systems (where the time evolution is unitary) one can predict such time averages without the need of calculating the dynamics. Since the wave function of any initial state can be written in terms of the eigenstates of the final Hamiltonian $|\Psi_{\alpha}\rangle$ as $|\psi_{ini}\rangle = \sum_{\alpha} C_{\alpha} |\Psi_{\alpha}\rangle$, one finds that the time evolution of the quantum

expectation value of an observable \hat{O} can be written as

$$\langle \hat{O}(\tau) \rangle \equiv \langle \psi(\tau) | \hat{O} | \psi(\tau) \rangle = \sum_{\alpha, \beta} C_{\alpha}^* C_{\beta} e^{i(E_{\alpha} - E_{\beta})\tau} O_{\alpha\beta}, \quad (8)$$

where $O_{\alpha\beta}$ are the matrix elements of \hat{O} in the basis of the final Hamiltonian. This in turn implies that the infinite time average of the observable can be written as

$$\overline{\langle \hat{O}(\tau) \rangle} \equiv O_{diag} = \sum_{\alpha} |C_{\alpha}|^2 O_{\alpha\alpha}. \quad (9)$$

We have assumed that, as in the case of generic (nonintegrable) systems, the spectrum is nondegenerate and incommensurate. This means that if the expectation value of \hat{O} relaxes to some kind of equilibrium value (up to the recurrences that must occur if the system is isolated), that value should be the one predicted by Eq. (9). Following previous work, we prefer to think of this exact result as the prediction of a ‘‘diagonal ensemble,’’ where $|C_{\alpha}|^2$ is the weight of each state within this ensemble [19, 25].

One objection that may arise at this point is that even if the system is nondegenerate and incommensurate, the spectrum may have arbitrarily close levels and it may take an unrealistically long time for the prediction in Eq. (9) to apply, i.e., that it may not be relevant to describe experiments. In order to study how the dynamics drives our observables of interest [$n(k)$ and $N(k)$] toward the prediction of Eq. (9), we follow the scheme in Ref. [25]. We study the normalized area between $n(k, \tau)$ and $N(k, \tau)$, during the time evolution, and their infinite time average, i.e., at different times we compute

$$\delta n_k(\tau) = \frac{\sum_k |n(k, \tau) - n_{diag}(k)|}{\sum_k n_{diag}(k)} \quad (10)$$

and

$$\delta N_k(\tau) = \frac{\sum_k |N(k, \tau) - N_{diag}(k)|}{\sum_k N_{diag}(k)} \quad (11)$$

In Fig. 1, we show results for $\delta n_k(\tau)$ and $\delta N_k(\tau)$ as a function of time τ for four different quenches as one approaches the integrable point. Besides undergoing the same change $t_{ini} = 0.5$, $V_{ini} = 2.0 \rightarrow t_{fin} = 1.0$, $V_{fin} = 1.0$, these quenches have another very important property in common. The initial state for each was selected to be one eigenstate of the initial Hamiltonian in such a way that the effective temperature T of the system [29] is always the same ($T = 2.0$ in Fig. 1). Given the energy of the time-evolving state in the final Hamiltonian, which is conserved,

$$E = \langle \psi_{ini} | \hat{H}_{fin} | \psi_{ini} \rangle, \quad (12)$$

the effective temperature T [29] is defined by the expression

$$E = \frac{1}{Z} \text{Tr} \left\{ \hat{H}_{fin} e^{-\hat{H}_{fin}/T} \right\}, \quad (13)$$

where

$$Z = \text{Tr} \left\{ e^{-\hat{H}_{fin}/T} \right\} \quad (14)$$

is the partition function, and we have set the Boltzmann constant k_B to unity, and $t_{fin} = 1$ sets the energy scale in our system.

In Figs. 1(a) and 1(f), we compare the initial momentum distribution and structure factors with the predictions of Eq. (9) away from integrability ($t' = V' = 0.32$). (The results for other values of t', V' are similar and not shown here.) The dynamics of those observables for four different values of t', V' is presented in Figs. 1(b)–1(e) for $\delta n_k(\tau)$ and in Figs. 1(g)–1(j) for $\delta N_k(\tau)$. They show that the dynamics of $n(k)$ and $N(k)$ are different. Away from integrability ($t' = V' \neq 0$), $\delta N_k(\tau)$ quickly relaxes [in a time scale $\tau \sim (t_{fin})^{-1} = 1.0$] to a value ~ 0.02 and then fluctuates around that value. $\delta n_k(\tau)$, on the other hand, slowly drifts toward $\delta n_k(\tau) \sim 0.02$ – 0.04 in a much longer time scale, orders of magnitude longer than the one seen for the relaxation of $\delta N_k(\tau)$.

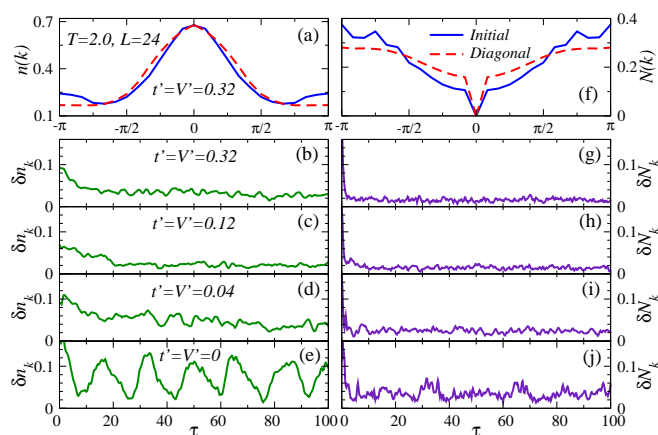


FIG. 1: (Color online) Quantum quench $t_{ini} = 0.5$, $V_{ini} = 2.0 \rightarrow t_{fin} = 1.0$, $V_{fin} = 1.0$, with $t'_{ini} = t'_{fin} = t'$ and $V'_{ini} = V'_{fin} = V'$ in a system with $N_f = 8$ and $L = 24$. The initial state was chosen in such a way that after the quench the system has an effective temperature $T = 2.0$ [29] in all cases. Given the energy of the initial state in the final Hamiltonian $E = \langle \psi_{ini} | \hat{H}_{fin} | \psi_{ini} \rangle$, the effective temperature is computed following Eq. (13). (a) Initial and diagonal ensemble results for $n(k)$ when $t' = V' = 0.32$. (b)–(e) Time evolution of δn_k for $t' = V' = 0.32, 0.12, 0.04$, and 0.0 , respectively. (f) Initial and diagonal ensemble results for $N(k)$ when $t' = V' = 0.32$. (g)–(j) Time evolution of δN_k for $t' = V' = 0.32, 0.12, 0.04$, and 0.0 , respectively.

The behavior of $\delta N_k(\tau)$ in these spin-polarized systems is qualitatively (and quantitatively) very similar to the one observed for hardcore bosons in Ref. [25]. The time evolution of δn_k for the fermions, on the other hand, is different from the one seen for the hardcore bosons in Ref. [25]. For the latter systems, $n(k)$ quickly relaxed toward the predictions of the diagonal ensemble, even at integrability. In Fig. 1(j), one can see that at integrability $\delta N_k(\tau)$ for the fermions also relaxes quickly toward the predictions of the diagonal ensemble and then exhibits fluctuations between $\delta N_k(\tau) = 0.02$ and $\delta N_k(\tau) = 0.06$, while $\delta n_k(\tau)$ in Fig. 1(e) exhibits very large oscillations between $\delta n_k(\tau) = 0.02$ and $\delta n_k(\tau) = 0.12$. Additionally, we studied the dynamics of δn_k for a time scale ten

times longer than the one depicted in Fig. 1(e) and observed exactly the same behavior.

For hardcore bosons [25], we have shown that increasing the effective temperature [29] (or the final energy E) decreases the mean value of $\delta n_k(\tau)$ and $\delta N_k(\tau)$ after relaxation and also decreases the temporal fluctuations of those quantities. In Fig. 2, we show results for quenches similar to the ones in Fig. 1, but with a higher effective temperature ($T = 3.0$). The comparison between Figs. 2 and 1 also reveals a reduction in the mean values of $\delta n_k(\tau)$ and $\delta N_k(\tau)$ and their fluctuations, which is particularly obvious at integrability. Still, differences remain between the relaxation dynamics of $\delta n_k(\tau)$ and $\delta N_k(\tau)$. Also, one can notice that at integrability the mean values of $\delta n_k(\tau)$ and $\delta N_k(\tau)$ and their fluctuations are in general larger than away from integrability, and they all decrease the further away one moves from the integrable point.

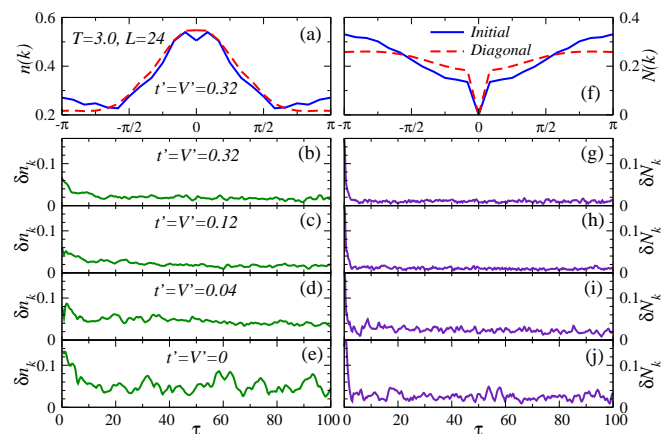


FIG. 2: (Color online) Quantum quench $t_{ini} = 0.5$, $V_{ini} = 2.0 \rightarrow t_{fin} = 1.0$, $V_{fin} = 1.0$, with $t'_{ini} = t'_{fin} = t'$ and $V'_{ini} = V'_{fin} = V'$ in a system with $N_f = 8$ and $L = 24$. The initial state was chosen in such a way that after the quench the system has an effective temperature $T = 3.0$ [29] in all cases (see the caption of Fig. 1). (a) Initial and diagonal ensemble results for $n(k)$ and $t' = V' = 0.32$. (b)–(e) Time evolution of δn_k for $t' = V' = 0.32, 0.12, 0.04$, and 0.0 , respectively. (f) Initial and diagonal ensemble results for $N(k)$ and $t' = V' = 0.32$. (g)–(j) Time evolution of δN_k for $t' = V' = 0.32, 0.12, 0.04$, and 0.0 , respectively.

The improvement of the relaxation dynamics with increasing the effective temperature (energy) of the isolated state [29], discussed above, can be related in part to the increase in the density of states in the final system with increasing energy. This increases the number of eigenstates of the Hamiltonian that participate in the dynamics making dephasing in Eq. (8) more effective, and hence reducing temporal fluctuations after relaxation. This can be better seen in Fig. 3, which clearly shows that the number of states with the largest values of $|C_\alpha|^2$ increases as the temperature decreases. Since $\sum_\alpha |C_\alpha|^2 = 1$, this means that the lower the temperature the smaller the total number of states that participate in the dynamics. This can be also seen in Fig. 3, where the number of states with $|C_\alpha|^2 > 10^{-5}$ and $|C_\alpha|^2 > 10^{-4}$ is larger for $T = 3.0$ [Fig. 3(b)] than for $T = 2.0$ [Fig. 3(a)] (notice the logarithmic scale in both axes). Overall, one can conclude that

dephasing becomes less effective with decreasing temperature and this leads to an enhancement of temporal fluctuations.

A similar argument, based on the number of states participating in the dynamics, can help us understand why the average values and temporal fluctuations of $\delta n_k(\tau)$ and $\delta N_k(\tau)$ are in general larger after relaxation when one is at integrability, or close to it. Figure 3 also shows that for any given temperature, the total number of states that participate in the dynamics decreases as one approaches the integrable point. At integrability, this may be related to the presence of additional conserved quantities, which restrict the number of eigenstates of the final Hamiltonian that can have a significant overlap with the initial state.

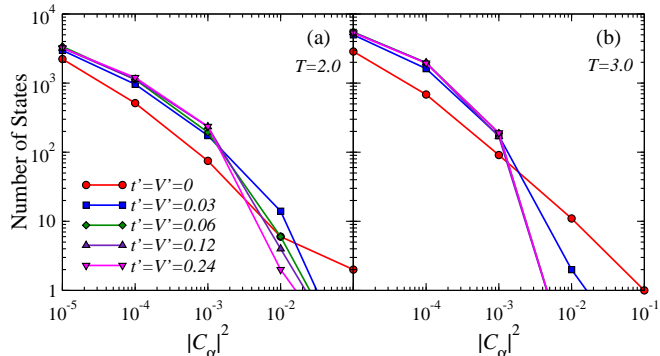


FIG. 3: (Color online) Number of states with $|C_\alpha|^2$ greater than the value presented in the x axis, for an effective temperature (a) $T = 2.0$ and (b) $T = 3.0$, and for the same quenches studied in Figs. 1 and 2, respectively. Here, $N_f = 8$ and $L = 24$.

It would be desirable to study how the mean values and temporal fluctuations of $\delta n_k(\tau)$ and $\delta N_k(\tau)$ behave after relaxation as one increases the system size. Unfortunately, the computational requirements of our approach increase exponentially with system size and a rigorous finite-size scaling is not possible. As a step in understanding how finite-size effects affect our results here, we show in Fig. 4 results for a smaller system with seven fermions in 21 lattice sites (with $T = 3.0$). By comparing those results with the ones in Fig. 2 one can see that, as expected, decreasing the system size increases the mean values of $\delta n_k(\tau)$ and $\delta N_k(\tau)$ after relaxation and the temporal fluctuations of both quantities. This supports the expectation that with increasing the system size, after relaxation, the mean values of $\delta n_k(\tau)$ and $\delta N_k(\tau)$ should become arbitrarily small and so should the temporal fluctuations.

A different question is what happens to the time scale for $n(k)$ to relax to the diagonal ensemble prediction as the system size increases. Previous work on that direction [30, 31] has suggested a possible intermediate quasisteady regime that occurs before full relaxation. This has been seen in recent numerical work [20], and our results for the behavior of $n(k)$ in smaller systems may be an indication in that direction. Something that is important to keep in mind from our results in this section is that different observables may exhibit different relaxation times. In particular, and in contrast to the hardcore boson case, the momentum distribution function of fermions is an observable that takes a long time to relax to an equilibrium distribution. This may have influenced the failure to

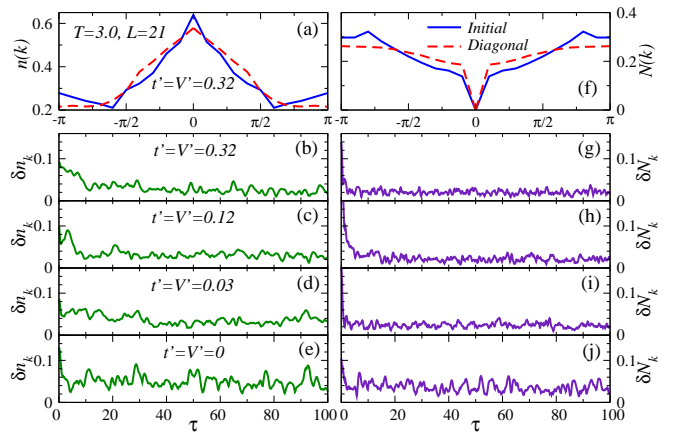


FIG. 4: (Color online) Quantum quench $t_{ini} = 0.5$, $V_{ini} = 2.0 \rightarrow t_{fin} = 1.0$, $V_{fin} = 1.0$, with $t'_{ini} = t'_{fin} = t'$ and $V'_{ini} = V'_{fin} = V'$ in a system with $N_f = 7$ and $L = 21$. The initial states were selected in the same way as the ones in Fig. 2 ($T = 3.0$). (a) Initial and diagonal ensemble results for $n(k)$ and $t' = V' = 0.32$. (b)–(e) Time evolution of δn_k for $t' = V' = 0.32, 0.12, 0.04$, and 0.0 , respectively. (f) Initial and diagonal ensemble results for $N(k)$ and $t' = V' = 0.32$. (g)–(j) Time evolution of δN_k for $t' = V' = 0.32, 0.12, 0.04$, and 0.0 , respectively.

observe thermalization in the momentum distribution function of a nonintegrable fermionic system in Ref. [23].

It is interesting to note that if $V = t' = V' = 0$ (noninteracting case) the momentum distribution function of fermions in a periodic system is a conserved quantity, i.e., for any initial state it will not change in time. However, the $n(k)$ of hardcore bosons, to which the fermions can be mapped, can have a nontrivial dynamics and relaxes to the predictions of a generalized Gibbs ensemble, as shown in Refs. [6] and [8]. Having $V, V' \neq 0$ (in our case $V = t = 1.0$ and V' varies between 0 and 0.32) allows the $n(k)$ of fermions to change with time (since now the fermions are interacting), but the time scale for relaxation to the equilibrium distribution still seems to be affected by the fact that in k space the scattering between fermions is very special. We find the relaxation time for $n(k)$ to be much longer than the corresponding time scale for other observables such as $N(k)$. The differences between the time scales for the relaxation of different observables (and their temporal fluctuations) can be understood in terms of the off-diagonal matrix elements of the observables, which will be discussed in Sec. VI.

IV. THERMODYNAMICS

In Sec. III, we have shown that, for our systems of interest, the diagonal ensemble provides an accurate description of observables after relaxation. Some observables may take longer to relax, and under some circumstances they may not even relax at all [see, e.g., $n(k)$ in Fig. 1(e)], but whenever we find relaxation to an equilibrium value, it is well described by the predictions of Eq. (9). This was expected and we refer the reader to Refs. [14, 19, 25] for similar results in other

quantum systems. In what follows, we study how the predictions of the diagonal ensemble compare to standard statistical mechanical ensembles. A great advantage of the infinite time average [Eq. (9)] is that all time dependence has been removed from the time evolution of the quantum-mechanical problem and one has a unique result to test statistical mechanics.

Since the systems on which we have performed the dynamics are isolated, the most appropriate statistical ensemble to compare observables after relaxation is the microcanonical ensemble. As usual, the computations in the microcanonical ensemble are performed averaging over all eigenstates (from all momentum sectors) that lie within a window $[E - \Delta E, E + \Delta E]$, where $E = \langle \psi_{ini} | \hat{H}_{fin} | \psi_{ini} \rangle$, and we have taken $\Delta E = 0.1$ in all cases. Similarly to what was done in Refs. [19] and [25], we have checked that our results are independent of the exact value of ΔE in the neighborhood of $\Delta E = 0.1$.

The main panel in Fig. 5(a) depicts how the difference between the diagonal and the microcanonical ensembles behaves as one moves away from integrability. Once again, we find a different behavior for $n(k)$ and $N(k)$. For $N(k)$, we find that for both effective temperatures [29] considered, the difference between the diagonal and microcanonical ensemble is always smaller than 1% for $t' = V' > 0.06$, and one can say that the system exhibits thermal behavior. This is very similar to the results for the same quantity obtained in the hardcore boson systems analyzed in Ref. [25]. On the other hand, $n(k)$ exhibits a larger difference between the diagonal and the microcanonical ensemble for the same values of t', V' , in particular at lower temperatures. For both observables, one can still see that as one approaches the integrable point, the difference between both ensembles increases, signaling the breakdown of thermalization in all cases.

In the inset in Fig. 5(a), we also compare the predictions of two diagonal ensembles generated by different initial states, which are chosen in such a way that the effective temperature of both system after the quench [29] are the same. The behavior is qualitatively similar to the one seen in the main panel of the same figure and shows that the breakdown of thermalization for both observables is accompanied by a dependence on the initial state.

Results for a smaller system size, with the same density and effective temperatures, are shown in the main panel and inset in Fig. 5(b). They show that, as expected, the differences between the two ensembles for any given value of t', V' increase with decreasing system size. Notice that the y axis in Figs. 5(a) and 5(b) has a different scale, so that the contrast between the results in both panels is stronger than may appear at first sight.

For $t' = V' > 0.06$, the comparison between the results for different systems sizes led us to expect that the predictions of the microcanonical ensemble, for both observables, will coincide with the ones of the diagonal ensemble as the system size is increased, i.e., that thermalization takes place if one is sufficiently far from integrability. We do note that $n(k)$ for these fermionic systems is more sensitive to finite-size effects than $N(k)$, something that is in contrast to the behavior seen for hardcore bosons [25].

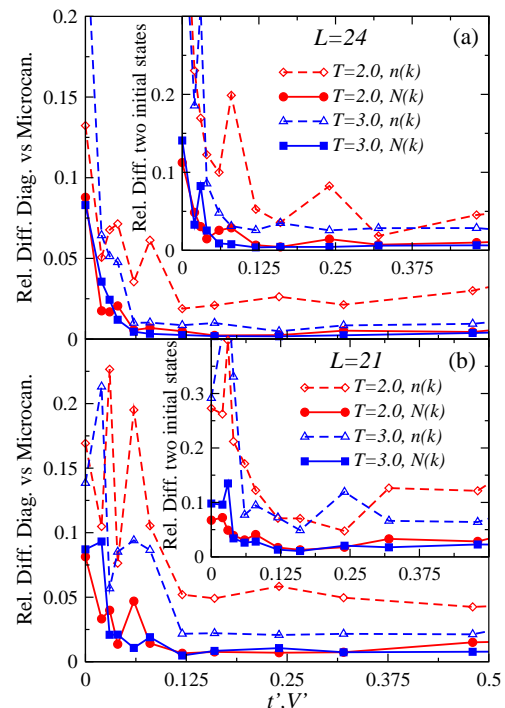


FIG. 5: (Color online) (Main panels) Comparison between the prediction of the microcanonical and diagonal ensembles, for $n(k)$ and $N(k)$, as a function of increasing t', V' for $T = 2.0$ and $T = 3.0$. Results are shown for (a) $L = 24$, $N_f = 8$, and (b) $L = 21$, $N_f = 7$. The diagonal ensembles correspond to the quenches in Figs. 1, 2, and 4. (Insets) Comparison between the prediction of diagonal ensembles generated by two different initial states, for $T = 2.0$ and $T = 3.0$. The results shown are for (a) $L = 24$, $N_f = 8$, and (b) $L = 21$, $N_f = 7$. As in the main panels, one of the diagonal ensembles is generated by initial states selected from the eigenstates of a Hamiltonian with $t_{ini} = 0.5$, $V_{ini} = 2.0$, the other diagonal ensemble is generated by initial states selected from the eigenstates of a Hamiltonian with $t_{ini} = 2.0$, $V_{ini} = 0.5$. The final Hamiltonian (with $t_{fin} = 1.0$, $V_{fin} = 1.0$) and the effective temperature [29] are identical for both initial states. By relative differences in this figure we mean the normalized area between the different ensemble predictions for $n(k)$ and $N(k)$. Relative differences are computed in exactly the same way as $\delta n_k(\tau)$ and $\delta N_k(\tau)$ are computed in Eqs. (10) and (11), respectively.

For values of $t' = V'$ closer to the $t' = V' = 0$ integrable point, the outcome of increasing system size is less clear, at least for the system sizes that we are able to analyze here. Two possibilities emerge. (i) As the system size increases the point at which the results for the diagonal and microcanonical ensembles start to differ will move toward $t' = V' = 0$. (ii) The very same point will move toward a nonzero value of t', V' . Here, we are not able to discriminate between those two scenarios, and further studies will be needed to address that question.

It is relevant to notice that, for the small systems sizes studied in this work, it is important to select the microcanonical ensemble when comparing with the outcome of the dynamics. This is because finite-size effects can make the predictions of different standard statistical mechanical ensembles differ-

ent from each other. In Fig. 6, we compare the results of the microcanonical ensemble, which we have been using up to this point, with the ones obtained with the canonical ensemble. One can see there that depending on the observable under consideration the results of both ensembles can differ up to $\sim 2.5\%$. The differences are not very much affected by the proximity to integrability, and, as expected, they can be seen to decrease with increasing system size. One can also see in Fig. 6 that the differences between the two ensembles are always larger for $n(k)$. Interestingly, they are not as large as the ones observed for the same quantity in the case of hardcore bosons [25].

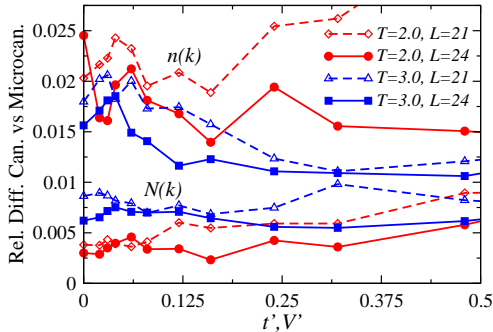


FIG. 6: (Color online) Relative differences (normalized area) between the predictions of the microcanonical and canonical ensembles for $n(k)$ [upper four curves] and $N(k)$ [lower four curves] in systems with $L = 21$, $N_f = 7$, and $L = 24$, $N_f = 8$. The relative differences are computed in exactly the same way as $\delta n_k(\tau)$ and $\delta N_k(\tau)$ are computed in Eqs. (10) and (11), respectively.

V. EIGENSTATE THERMALIZATION HYPOTHESIS

In what follows, we will analyze the reason underlying thermalization in these isolated quantum systems, and the cause for the differences seen between $n(k)$ and $N(k)$ when comparing the diagonal and microcanonical ensembles.

In Sec. IV, we have shown that away from integrability there are regimes in which the system thermalizes, i.e., in which the predictions of the diagonal ensemble and the microcanonical ensemble coincide. This means that

$$O_{diag} = O_{microc},$$

$$\sum_{\alpha} |C_{\alpha}|^2 O_{\alpha\alpha} = \frac{1}{\mathcal{N}_{E, \Delta E}} \sum_{|E-E_{\alpha}| < \Delta E} O_{\alpha\alpha}, \quad (15)$$

where $\mathcal{N}_{E, \Delta E}$ is the number of energy eigenstates with energies in the window $[E - \Delta E, E + \Delta E]$. This result is certainly surprising because the left-hand side of Eq. (15) depends on the initial conditions through the overlaps of the initial state with the eigenstates of the final Hamiltonian (C_{α}), while the right-hand side of Eq. (15) only depends on the energy E (as mentioned before, our results do not depend on the specific value of ΔE).

A possible solution to this paradox was advanced by Deutsch [21] and Srednicki [22] in terms of the eigenstate

thermalization hypothesis (ETH). Within ETH, the difference between the eigenstate expectation values of generic few-body observables [$O_{\alpha\alpha}$] are presumed to be small between eigenstates that are close in energy. This implies that if one takes a small window of energy ΔE , as it is done in the microcanonical ensemble, all the eigenstate expectation values within that window will be very similar to each other. Hence, the microcanonical average and a single eigenstate will provide essentially the same answer, i.e., the eigenstates already exhibit thermal behavior. The same will happen with the prediction of the diagonal ensemble as long as the $|C_{\alpha}|$'s are strongly peaked around the energy E . The latter has been shown to be the case for quenches in hardcore boson systems in two dimensions [19], hardcore bosons in one dimension [25, 32], softcore bosons in one dimension [33], and generic quenches in the thermodynamic limit [19].

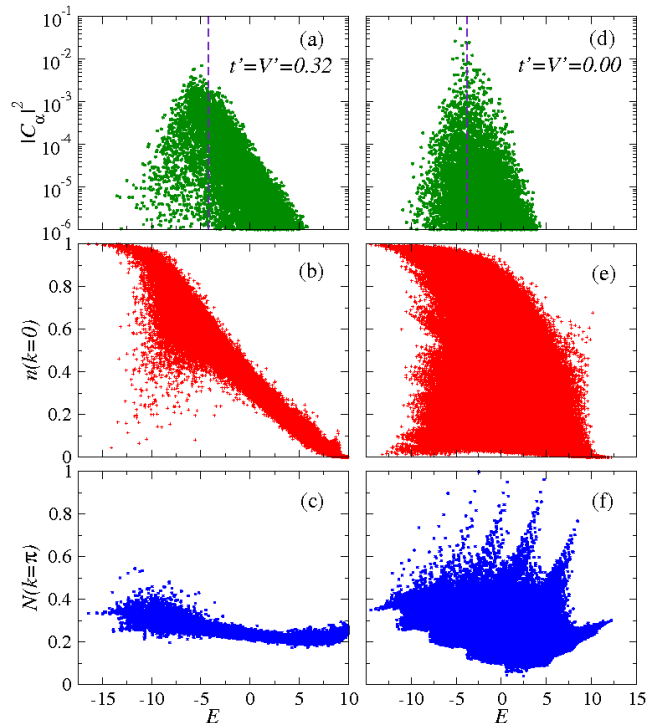


FIG. 7: (Color online) (a),(d) Distribution of $|C_{\alpha}|^2$ for two of the quenches depicted in Fig. 2, for (a) $t'_{fin} = V'_{fin} = 0.32$ and (d) $t'_{fin} = V'_{fin} = 0.0$. In both cases, the final effective temperature of the system is $T = 3.0$ [29]. The vertical dashed lines signal the energy E of the time-evolving state. (b),(e) Eigenstate expectation values of $\hat{n}(k=0)$ in the full spectrum (including all momentum sectors) of the Hamiltonian (1) with $t = V = 1.0$ and, (b) $t' = V' = 0.32$ and (e) $t' = V' = 0.0$. (c),(f) Eigenstate expectation values of $\hat{N}(k=\pi)$ in the full spectrum (including all momentum sectors) of the Hamiltonian (1) with $t = V = 1.0$ and, (c) $t' = V' = 0.32$ and (f) $t' = V' = 0.0$. These results were obtained for systems with $L = 24$ and $N_f = 8$, i.e., the total Hilbert space consists of 735 471 states.

In Figs. 7(a) and 7(d), we show the distributions of $|C_{\alpha}|^2$ for two of the quenches studied in Fig. 2. One quench is far away from integrability and the other one at integrability. There are some features of the distributions of $|C_{\alpha}|^2$ that are important to mention here. (i) They are neither similar to the

microcanonical nor to the canonical distributions. (ii) They are strongly peaked around the energy E of the time-evolving state. Actually, one can see in the figures that the values of $|C_\alpha|^2$ decay exponentially as one moves away from E (signaled by the vertical line in the figures). (iii) They are not related to the effective temperature of the system, which is exactly the same in both cases ($T = 3.0$) while the distributions of $|C_\alpha|^2$ are clearly different. The specific values of $|C_\alpha|^2$, and the exponent of their decay, depend on the initial state [32]. Because of these properties of the $|C_\alpha|^2$ distributions, they alone cannot explain why thermalization takes place, for example, for $N(k)$ when $t' = V' = 0.32$ in Fig. 5.

In the bottom four panels of Fig. 7, we show the eigenstate expectation values of $\hat{n}(k=0)$ [(b),(e)] and $\hat{N}(k=\pi)$ [(c),(f)] for a system far from integrability, with $t = V = 1.0$ and $t' = V' = 0.32$ [(b),(c)], and for a system at integrability, with $t = V = 1.0$ and $t' = V' = 0.0$ [(e),(f)]. Those results, together with the $|C_\alpha|^2$ distributions in Figs. 7(a) and 7(d), can help us understand the differences between the diagonal and the microcanonical ensembles in Fig. 5(a).

The most striking feature in the bottom panels in Fig. 7 is the contrast between the eigenstate expectation values at integrability and far away from it. The former ones exhibit a very wide distribution of eigenstate expectation values. This is true even if one selects a narrow window at the center of the spectrum (equivalent to very high temperatures). As one moves away from integrability, one can clearly see that the fluctuations between eigenstate expectation values of nearby eigenstates reduces dramatically and ETH starts to be valid. For $t' = V' = 0.32$, a comparison between the expectation values of $\hat{n}(k=0)$ and $\hat{N}(k=\pi)$ shows that for the energies of the final states created in our quenches, the distribution of the eigenstate expectation values of $\hat{n}(k=0)$ is relatively broader than the one seen for $\hat{N}(k=\pi)$, which explains why the differences between the diagonal and microcanonical ensembles in Fig. 5(a) are larger for the former one. It also helps in understanding why $\hat{n}(k)$ is more sensitive to the selection of the initial state.

In order to gain a more quantitative understanding of how ETH breaks down as one approaches integrability, we have computed the average relative deviation of the eigenstate expectation values with respect to the microcanonical prediction, $\Delta^{mic}n(k=0)$ and $\Delta^{mic}N(k=\pi)$. For any given energy of the microcanonical ensemble, these quantities are computed as

$$\Delta^{mic}n(k=0) = \frac{\sum_\alpha |n_{\alpha\alpha}(k=0) - n_{mic}(k=0)|}{\sum_\alpha n_{\alpha\alpha}(k=0)} \quad (16)$$

and

$$\Delta^{mic}N(k=\pi) = \frac{\sum_\alpha |N_{\alpha\alpha}(k=\pi) - N_{mic}(k=\pi)|}{\sum_\alpha N_{\alpha\alpha}(k=\pi)} \quad (17)$$

where $n_{\alpha\alpha}(k=0)$ and $N_{\alpha\alpha}(k=\pi)$ are the eigenstate expectation values of $\hat{n}(k=0)$ and $\hat{N}(k=\pi)$, respectively, and $n_{mic}(k=0)$ and $N_{mic}(k=\pi)$ are the microcanonical expectation values at any given energy E . The sum over α contains

all states with energies in the window $[E - \Delta E, E + \Delta E]$. As discussed before, we have taken $\Delta E = 0.1$.

Clearly, for different values of the Hamiltonian parameters, the lowest and highest-energy states as well as the level spacing are different. Hence, in order to make a meaningful comparison between different systems as one moves away from the integrable point, we study the behaviors of $\Delta^{mic}n(k=0)$ and $\Delta^{mic}N(k=\pi)$ as a function of the effective temperature T of a canonical ensemble that has the same energy E as the microcanonical ensemble. Given an energy E within the microcanonical ensemble, the effective temperature can be computed by means of Eq. (13). We should stress that the effective temperature is only used here as an auxiliary tool for comparing different systems, i.e., it just provides a unique energy scale for comparing observables independently of the Hamiltonian parameters, which change the ground-state energy and the level spacing.

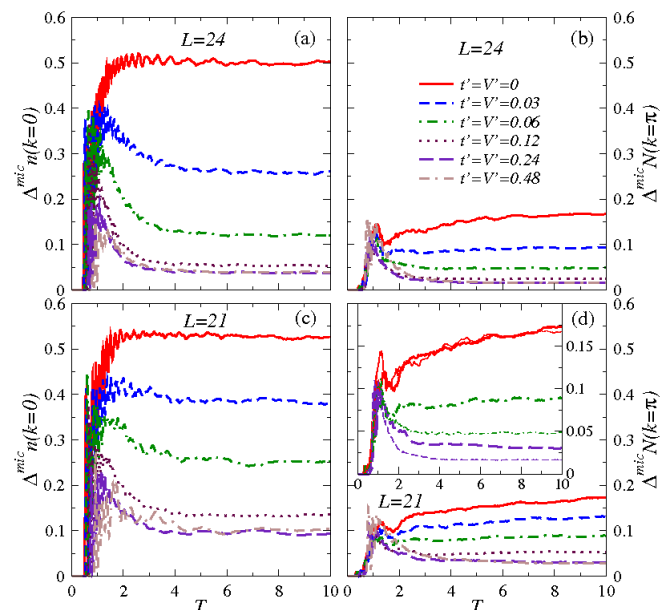


FIG. 8: (Color online) Average relative deviation of eigenstate expectation values with respect to the microcanonical prediction vs T (see text). Results are presented for: (a),(c) $\Delta^{mic}n(k=0)$ and (b),(d) $\Delta^{mic}N(k=\pi)$ in systems with: (a),(b) $L = 24$, $N_f = 8$ and (c),(d) $L = 21$, $N_f = 7$. The inset in (d) shows a direct comparison of $\Delta^{mic}N(k=\pi)$ between the systems with $L = 24$, $N_f = 8$ (thin lines) and the systems with $L = 21$, $N_f = 7$ (thick lines). The values of t', V' in the three cases depicted in the inset are, from top to bottom, $t' = V' = 0$, $t' = V' = 0.06$, and $t' = V' = 0.24$, and follow the same legends of the main panel shown in (b). In all cases $t = V = 1.0$.

In Fig. 8, we present results for $\Delta^{mic}n(k=0)$ [(a),(c)] and $\Delta^{mic}N(k=\pi)$ [(b),(d)] vs T for six different values of $t' = V'$ in systems with 24 lattice sites and eight fermions [(a),(b)] and 21 lattice sites and seven fermions [(c),(d)]. The average relative deviations for both observables are presented in the same scale, which immediately allows one to see what was already evident in Fig. 7, namely, that the average relative deviations for $\Delta^{mic}n(k=0)$ are larger (more than two times larger) than the corresponding ones for $\Delta^{mic}N(k=\pi)$ for

any given value of t', V' . For temperatures $T \gtrsim 1.5$, one can see that those deviations for both observables saturate with increasing t', V' for $t' = V' > 0.12$. Comparing the results for the same observables but for different systems sizes, one can see that with increasing system size the average relative deviations are decreasing. This can be better seen in the inset in Fig. 8(d), where we have presented a direct comparison of $\Delta^{mic} N(k = \pi)$ for three different values of t', V' in the systems with 21 (thick lines) and 24 (thin lines) sites. At integrability, one does not see much of a change with changing system size for $\Delta^{mic} N(k = \pi)$, but some reduction can be seen for $\Delta^{mic} n(k = 0)$ [Figs. 8(a) and 8(c)]. For $t' = V' > 0$, we do see a clear reduction in all cases. At low temperatures $T < 1.5$, the density of states is low and in many cases the use of the microcanonical ensemble is not justified. From Fig. 7, one can see that in that regime (of low energies) the fluctuations of the observables are very large and thermalization is not expected to occur. An important question that needs to be addressed in the future is what will happen with that window of temperatures (energies) with increasing the system size. For our small systems, we do not see a noticeable change with increasing system size.

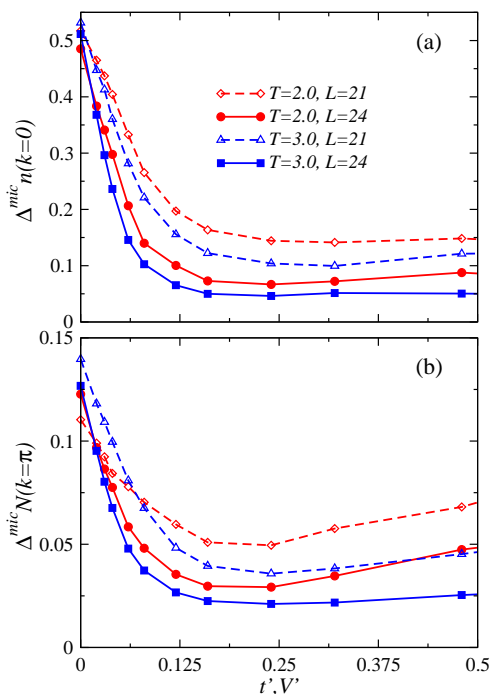


FIG. 9: (Color online) Average relative deviation of eigenstate expectation values with respect to the microcanonical prediction at two fixed temperatures ($T = 2.0$ and $T = 3.0$) and for two system sizes ($L = 21$, $N_f = 7$, and $L = 24$, $N_f = 8$) vs t', V' . Results are presented for: (a) $\Delta^{mic} n(k = 0)$ and (b) $\Delta^{mic} N(k = \pi)$. In all cases $t = V = 1.0$.

An alternative way to present some of the results depicted in Fig. 8, which can help us make direct contact with the results discussed in Fig. 5, is to take two values of the effective temperature within the microcanonical ensemble and plot the average relative deviation of eigenstate expectation values with respect to the microcanonical prediction for those tem-

peratures as a function of the integrability breaking parameters t', V' . This is done in Fig. 9 for $T = 2.0$ and $T = 3.0$, and $L = 21$ and $L = 24$. Figure 9 clearly shows that the breakdown of thermalization seen in Fig. 5 as one approaches integrability is directly related to the increase in the relative deviation of eigenstate expectation values with respect to the microcanonical prediction, i.e., to the increase in the fluctuations of the eigenstate to eigenstate expectation values of $\hat{n}(k)$ and $\hat{N}(k)$, or what is the same to the failure of ETH. A comparison between Figs. 9(a) and 9(b) also helps in understanding why in Fig. 5 the difference between the diagonal and microcanonical ensembles is larger for $n(k)$ than for $N(k)$, even when one is far from integrability. Figure 9(a) shows that for the effective temperatures selected in Fig. 5, $\Delta^{mic} n(k = 0)$ is more than two times larger than $\Delta^{mic} N(k = \pi)$. The reduction in $\Delta^{mic} n(k = 0)$ and $\Delta^{mic} N(k = \pi)$, with increasing system size, can also be seen in Fig. 9 when comparing the results for $L = 21$ and $L = 24$.

VI. OFF-DIAGONAL MATRIX ELEMENTS

While the diagonal elements of the observables, in the basis of the eigenstates of the Hamiltonian, helped us understand whether after relaxation the expectation values of generic few-body observables can be described by standard statistical mechanical approaches, it follows from Eqs. (8) and (9) that the off-diagonal elements of the observables can help us understand the relaxation dynamics and temporal fluctuations of observables after relaxation,

$$\langle \hat{O}(\tau) \rangle - \overline{\langle \hat{O}(\tau) \rangle} = \sum_{\substack{\alpha\beta \\ \alpha \neq \beta}} C_\alpha^* C_\beta e^{i(E_\alpha - E_\beta)\tau} O_{\alpha\beta}. \quad (18)$$

As we pointed out in Sec. III, one of our findings in this work is that the momentum distribution function of fermions exhibits a slower relaxation dynamics than the one seen for the same observable in an identical system of hardcore bosons [25]. These differences were seen far from the integrable point as well as at the integrable point. In Figs. 10(a) and 10(c), we compare the off-diagonal elements of $\hat{n}(k = 0)$ between a system of spinless fermions [Fig. 10(a)] and an identical system with hardcore bosons [Fig. 10(c)], both systems are far from integrability [with $t' = V' = 0.32$] and the central eigenstate has an energy for which the temperature of a canonical ensemble with the same energy would be $T = 3.0$. It is apparent in these two figures that the off-diagonal elements of $\hat{n}(k = 0)$ are larger for the fermions than for the hardcore bosons, in particular close to the diagonal.

The relaxation dynamics of our other observable of interest $N(k)$, on the other hand, was seen to be very similar between the fermions studied in this work and the hardcore bosons studied in Ref. [25]. In both systems, this observable relaxed very quickly (in a time scale $\tau \sim 1/t$). Figures 10(b) and 10(d) depict results for the off-diagonal elements of $\hat{N}(k = \pi)$. The results for fermions and hardcore bosons are almost indistinguishable in this case, with all off-diagonal elements being much smaller than the diagonal ones. The con-

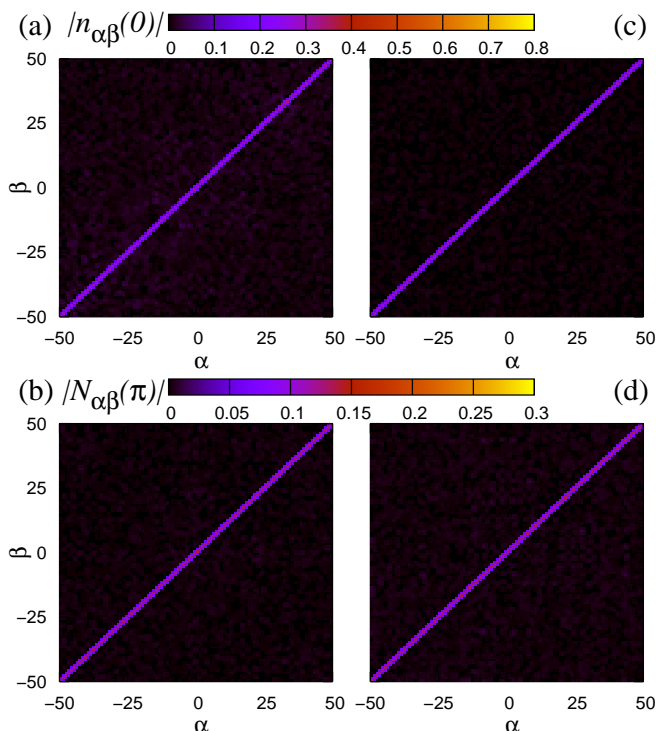


FIG. 10: (Color online) Off-diagonal elements of $\hat{n}(k=0)$ [(a),(c)] and $\hat{N}(k=\pi)$ [(b),(d)] for fermions [(a),(b)] and hardcore bosons [(c),(d)] far from integrability. Results are shown for the 100 eigenstates closest to the one with energy $E = -4.26$ ($T = 3.0$, see text) for the fermions [(a),(b)] and $E = -4.62$ ($T = 3.0$, see text) for the hardcore bosons [(c),(d)]. In all cases $t = V = 1.0$, $t' = V' = 0.32$, $L = 24$, and $N_f = N_b = 8$.

trast between the magnitude of the off-diagonal elements of $\hat{n}(k=0)$ in Fig. 10(a) and $\hat{N}(k=\pi)$ in Fig. 10(b) also explains the difference between the relaxation dynamics of both observables in fermionic systems depicted in Fig. 1.

Results for the same quantities for fermions and hardcore bosons at the integrable point are shown in Fig. 11. We find the results at integrability in stark contrast with those far away from the integrable point. At integrability, the off-diagonal elements of both observables are in most cases very small or zero, but then there are some states between which the off-diagonal elements can be very large (much larger than any off-diagonal element seen in the nonintegrable case). In addition, very large off-diagonal elements can be seen between states that have quite different energies. In Fig. 10, the largest off-diagonal elements in the nonintegrable case always occur between states that are close in energies, and they are seen to reduce as the energy of the states depart from each other. This is not the case at integrability.

A more quantitative understanding of these issues can be gained by taking one state from Figs. 10 and 11 and plotting the off-diagonal elements between that state (which we take to be the one at the center) and all the closest energy eigenstates for our two observables of interest. These are depicted in Fig. 12 for the nonintegrable case with $t' = V' = 0.32$ [(a)–(c)] and at integrability $t' = V' = 0$ [(d)–(f)].

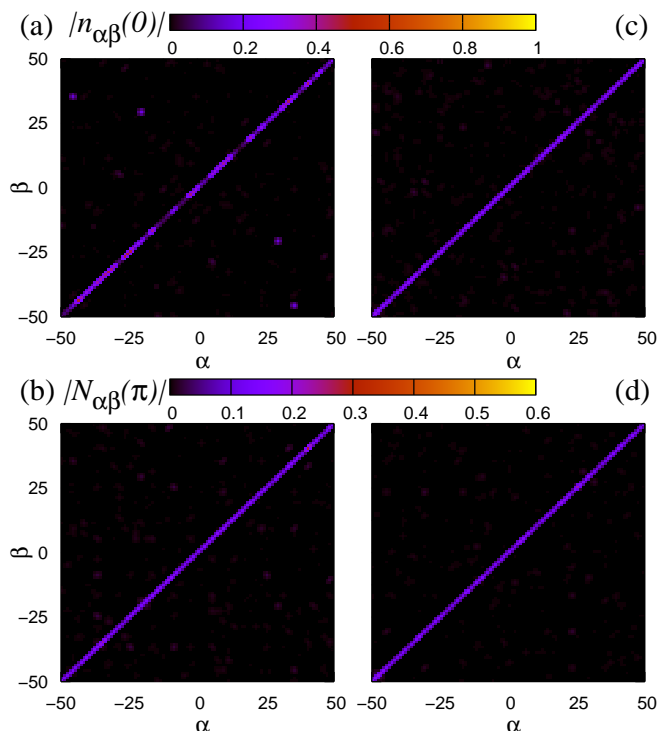


FIG. 11: (Color online) Off-diagonal elements of $\hat{n}(k=0)$ [(a),(c)] and $\hat{N}(k=\pi)$ [(b),(d)] for fermions [(a),(b)] and hardcore bosons [(c),(d)] at integrability. Results are shown for the 100 eigenstates closest to the one with energy $E = -3.84$ ($T = 3.0$, see text) for the fermions [(a),(b)] and $E = -3.84$ ($T = 3.0$, see text) for the hardcore bosons [(c),(d)]. In all cases $t = V = 1.0$, $t' = V' = 0.00$, $L = 24$, and $N_f = N_b = 8$.

First, let us focus on the behavior of $n_{\alpha\beta}(k=0)$. Results for that quantity in the nonintegrable fermionic and hardcore boson cases are shown in panels (a) and (b) for two lattices with $L = 21$ and $L = 24$, respectively. For each lattice size, one can clearly see that the off-diagonal elements of $\hat{n}(k=0)$ of the fermions are always larger than the ones of the bosons, and the differences are largest close to the diagonal. As the energies between the states depart from each other $n_{\alpha\beta}(k=0)$ for bosons and fermions become similar. The comparison between the two lattices also shows that with increasing system size the off-diagonal elements of the observables decrease, but the fact that $n_{\alpha\beta}(k=0)$ for the fermions is larger close to the diagonal remains. Similarly, we find that with decreasing the energy of the state the off-diagonal elements of $n_{\alpha\beta}(k=0)$ also become larger, although for temperatures $T > 1.0$ this effect is smaller than the finite-size effect difference between panels (a) and (b) in Fig. 12.

Results for $n_{\alpha\beta}(k=0)$ at integrability are presented in panels (d) and (e) of Fig. 12. There one can also see that the values of $n_{\alpha\beta}(k=0)$ are in general larger for fermions than for hardcore bosons and that they decrease with increasing the system size. However, here fermions and bosons share a common feature, namely, large off-diagonal elements can be seen between states that have energies that are increasingly different from each other. This, in conjunction with the fewer number of states that have a significant overlap with the ini-

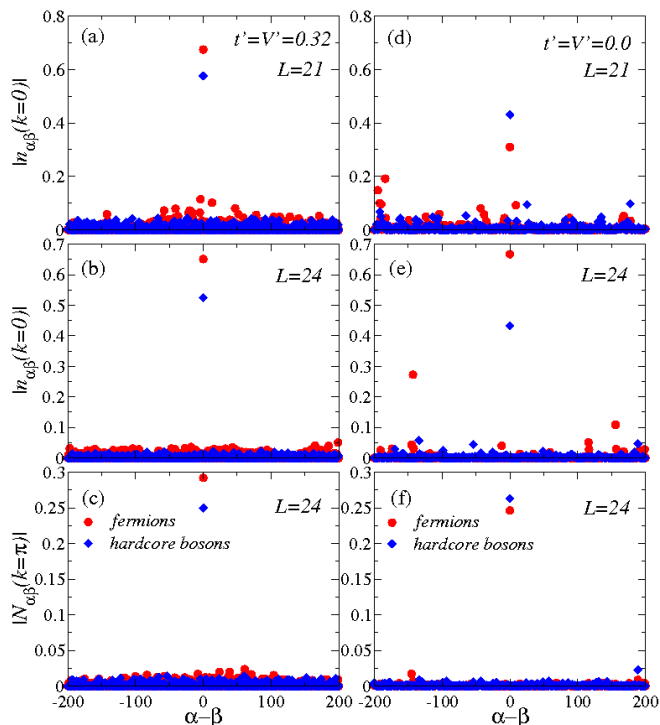


FIG. 12: (Color online) Off-diagonal elements of $\hat{n}(k = 0)$ [(a),(b),(d),(e)] and $\hat{N}(k = \pi)$ [(c),(f)] for fermions and hardcore bosons away from integrability [(a)–(c)] and at integrability [(d)–(f)]. Panels (b),(c),(e),(f) correspond to cuts across Figs. 10 and 11, with either $\alpha = 0$ or $\beta = 0$. Panels (a) and (d) depict results for the off-diagonal elements of $\hat{n}(k = 0)$ in systems with $L = 21$. In all cases, the eigenstate defining the center of the window has the energy closest to that of a canonical ensemble with temperature $T = 3.0$.

tial state, can lead to larger temporal fluctuations during the time evolution after a quench at integrability. This effect is enhanced at lower temperatures where we see some increase in the magnitude of the off-diagonal elements and a decrease in the number of states that overlap with the initial state (see Fig. 3).

Finally, the off-diagonal elements for $\hat{N}(k = \pi)$ far from integrability and at integrability are presented in Fig. 12, panels (c) and (f), respectively. Those panels show that, for the density-density structure factor, off-diagonal elements are always much smaller than the diagonal ones, and they are relatively smaller than the ones of $\hat{n}(k)$. At integrability [Fig. 12(f)], one can see a few values of $N_{\alpha\beta}(k = \pi)$ that are clearly larger than the rest, but they are still less and relatively smaller than the ones seen for $n_{\alpha\beta}(k = 0)$ in Fig. 12(e). These results explain why $\hat{N}(k)$ takes less time to relax to the diagonal ensemble prediction and why the temporal fluctuations after relaxation are also smaller for this observable.

VII. SUMMARY

We have presented a detailed study of the relaxation dynamics after a quantum quench and the description after re-

laxation of the momentum distribution function $n(k)$ (a one-particle observable) and the density-density structure factor $N(k)$ (a two-particle observable) of spinless fermions with nearest and next-nearest hoppings and interactions in one-dimensional periodic lattices. We have also compared some results for fermions with those of a similar hardcore boson system. We should stress that those models are typical for describing the physics of one-dimensional systems. For example, they can be mapped onto the spin-1/2 XXZ linear chain with next-nearest-neighbor interactions. (The observables analyzed here are related to the different spin-spin correlation functions.) Hence, we expect the results reported in this manuscript to be generic and apply to other gapless models and observables in one-dimensional systems.

We have shown that, in general, $n(k)$ for fermions exhibits a slower relaxation dynamics, i.e., it takes longer to relax to an equilibrium distribution than other observables for fermions [such as $N(k)$] and than $n(k)$ for a similar one-dimensional system of hardcore bosons (studied in Ref. [25]). Close to and at integrability, we have also found that $n(k)$ may even fail to relax to an equilibrium distribution while $N(k)$, and $n(k)$ for a similar bosonic system, do relax to equilibrium. We have shown that this behavior of the dynamics of $n(k)$ is related to the particularly large off-diagonal elements of $\hat{n}(k)$ in the basis of the eigenstates of the Hamiltonian. Those off-diagonal elements are larger than the ones for the same observable in hardcore boson systems, and much larger than the ones for $\hat{N}(k)$ in the same fermionic system. From the contrast between the dynamics of $n(k)$ and $N(k)$ emerges a general picture in which some few-body observables in isolated quantum systems may quickly relax to an equilibrium distribution while other observables may take longer to relax, or even fail to relax, to an equilibrium distribution.

We have shown that far from integrability observables after relaxation are well described by standard ensembles from statistical mechanics, such as the microcanonical ensemble, which is particularly relevant to our small and isolated systems. The ability of the microcanonical ensemble to predict the expectation value of few-body observables after relaxation was shown to be related to the validity of the eigenstate thermalization hypothesis, within which the expectation values of observables in the eigenstates of the Hamiltonian already exhibit thermal behavior. We have also shown that as one approaches the integrable point thermalization breaks down, with the differences between the microcanonical predictions and the results of the relaxation dynamics increasing continuously as one converges toward the integrable point. We have established that there is a clear correlation between the failure of the system to thermalize and the failure of the eigenstate thermalization hypothesis, i.e., as one approaches integrability the differences between the eigenstate expectation values of few-body observables increases between eigenstates that are close in energy, and this happens over the full spectrum of the Hamiltonian.

Our results here have been obtained for small one-dimensional lattices, which are relevant to current experiments in one-dimensional geometries [34]. However, several important questions remain to be addressed in future works.

For example, what happens to the point at which thermalization breaks down (at all temperatures) as one increases the system size. Far from integrability, we find that for our small systems thermalization occurs whenever the effective temperature is $T \gtrsim 1.5$ [29]. Another question that needs to be addressed is what happens with the window of energies where thermalization fails to occur far from integrability as one increases the system size. Finally, there is the question of the time scale that $n(k)$ of the fermions takes to relax to the thermal distribution, and the emergence of intermediate quasistationary distributions [30, 31], as the size of the system is increased. Experiments with ultracold gases will generate many

new questions and help address the current ones.

Acknowledgments

This work was supported by the U.S. Office of Naval Research under Award No. N000140910966 and by a Summer Academic Grant from Georgetown University. We thank Amy Cassidy and Itay Hen for useful comments on the manuscript. We are grateful to the Aspen Center for Physics for hospitality.

-
- [1] M. Greiner, O. Mandel, T. W. Hänsch, and I. Bloch, *Nature (London)* **419**, 51 (2002).
- [2] T. Stöferle, H. Moritz, C. Schori, M. Köhl, and T. Esslinger, *Phys. Rev. Lett.* **92**, 130403 (2004).
- [3] H. Ott, E. de Mirandes, F. Ferlaino, G. Roati, G. Modugno, and M. Inguscio, *Phys. Rev. Lett.* **92**, 160601 (2004).
- [4] C. D. Fertig, K. M. O'Hara, J. H. Huckans, S. L. Rolston, W. D. Phillips, and J. V. Porto, *Phys. Rev. Lett.* **94**, 120403 (2005).
- [5] T. Kinoshita, T. Wenger, and D. S. Weiss, *Nature (London)* **440**, 900 (2006).
- [6] M. Rigol, V. Dunjko, V. Yurovsky, and M. Olshanii, *Phys. Rev. Lett.* **98**, 050405 (2007).
- [7] S. Hofferberth, I. Lesanovsky, B. Fischer, T. Schumm, and J. Schmiedmayer, *Nature (London)* **449**, 324 (2007).
- [8] M. Rigol, A. Muramatsu, and M. Olshanii, *Phys. Rev. A* **74**, 053616 (2006).
- [9] M. A. Cazalilla, *Phys. Rev. Lett.* **97**, 156403 (2006).
- [10] P. Calabrese and J. Cardy, *J. Stat. Mech.* p. P06008 (2007).
- [11] M. Cramer, C. M. Dawson, J. Eisert, and T. J. Osborne, *Phys. Rev. Lett.* **100**, 030602 (2008).
- [12] T. Barthel and U. Schollwöck, *Phys. Rev. Lett.* **100**, 100601 (2008).
- [13] M. Eckstein and M. Kollar, *Phys. Rev. Lett.* **100**, 120404 (2008).
- [14] M. Kollar and M. Eckstein, *Phys. Rev. A* **78**, 013626 (2008).
- [15] M. Cramer, A. Flesch, I. P. McCulloch, U. Schollwöck, and J. Eisert, *Phys. Rev. Lett.* **101**, 063001 (2008).
- [16] A. Flesch, M. Cramer, I. P. McCulloch, U. Schollwöck, and J. Eisert, *Phys. Rev. A* **78**, 033608 (2008).
- [17] D. Rossini, A. Silva, G. Mussardo, and G. Santoro, *Phys. Rev. Lett.* **102**, 127204 (2009).
- [18] A. Iucci and M. A. Cazalilla, arXiv:0903.1205.
- [19] M. Rigol, V. Dunjko, and M. Olshanii, *Nature (London)* **452**, 854 (2008).
- [20] M. Eckstein, M. Kollar, and P. Werner, *Phys. Rev. Lett.* **103**, 056403 (2009).
- [21] J. M. Deutsch, *Phys. Rev. A* **43**, 2046 (1991).
- [22] M. Srednicki, *Phys. Rev. E* **50**, 888 (1994).
- [23] S. R. Manmana, S. Wessel, R. M. Noack, and A. Muramatsu, *Phys. Rev. Lett.* **98**, 210405 (2007).
- [24] C. Kollath, A. M. Läuchli, and E. Altman, *Phys. Rev. Lett.* **98**, 180601 (2007).
- [25] M. Rigol, *Phys. Rev. Lett.* **103**, 100403 (2009).
- [26] A. K. Zhuravlev, M. I. Katsnelson, and A. V. Trefilov, *Phys. Rev. B* **56**, 12939 (1997).
- [27] P. Jordan and E. Wigner, *Z. Phys.* **47**, 631 (1928).
- [28] E. Altman, E. Demler, and M. D. Lukin, *Phys. Rev. A* **70**, 013603 (2004).
- [29] By the effective temperature (T), we mean the temperature of a canonical ensemble with the same energy as the (isolated) time-evolving state. This temperature help us gauge the excitation energy of the time-evolving state with respect to the ground state. In addition, in thermodynamics systems where observables are expected to thermalize, T allows one to predict the expectation values of observables of interest after relaxation.
- [30] M. Moeckel and S. Kehrein, *Phys. Rev. Lett.* **100**, 175702 (2008).
- [31] M. Moeckel and S. Kehrein, *Ann. Phys.* **324**, 2146 (2009).
- [32] M. Rigol, arXiv:0909.4556 (2009).
- [33] G. Roux, *Phys. Rev. A* **79**, 021608(R) (2009).
- [34] B. Paredes, A. Widera, V. Murg, O. Mandel, S. Fölling, I. Cirac, G. V. Shlyapnikov, T. W. Hänsch, and I. Bloch, *Nature (London)* **429**, 277 (2004).